Construction of multi-walled carbon nanotubes/$ZnSnO_3$ heterostructures for enhanced acetone sensing performance

Liyong Du(杜丽勇)[1,†] and Heming Sun(孙鹤鸣)[2]

[1] *Department of Materials and Chemical Engineering, Taiyuan University, Taiyuan* 030032, *China*
[2] *College of Physics, Jilin University, Changchun* 130012, *China*

(Received 7 June 2022; revised manuscript received 10 August 2022; accepted manuscript online 16 August 2022)

Carbon nanotubes (CNTs) have attracted many researcher's attention in gas sensing field because of their excellent physical and chemical properties. Herein, multi-walled carbon nanotubes (MWCNTs)/$ZnSnO_3$ heterostructures have been obtained by a simple hydrothermal method without additional annealing process. The structural and composition information are characterized by x-ray diffraction (XRD), field-emission scanning electron microscopy (FESEM), transmission electron microscopy (TEM) and x-ray photoelectron spectroscopy (XPS). The acetone sensing properties of pure MWCNTs, $ZnSnO_3$ and MWCNTs/$ZnSnO_3$ heterostructures are systematically investigated, respectively. The results show that MWCNTs/$ZnSnO_3$ heterostructures have better sensing properties compared with pure MWCNTs and $ZnSnO_3$ sample. Specifically, MWCNTs/$ZnSnO_3$ heterostructures exhibit not only high responses of 24.1 and rapid response/recovery speed of 1 s/9 s to 100 ppm acetone, but also relatively good repeatability and long-term stability. The enhanced sensing performance is analyzed in detail. In addition, this work provides the experimental and theory basis for synthesis of high-performance MWCNT-based chemical sensors.

Keywords: carbon nanotube, $ZnSnO_3$, p–n heterostructures, acetone

PACS: 07.07.Df, 68.47.Gh, 73.40.Lq **DOI:** 10.1088/1674-1056/ac89da

1. Introduction

Acetone, also known as dimethyl ketone, is a colorless transparent liquid with a special pungent smell. It has been widely used in many fields including industry, agriculture and medicine and so on.[1] However, acetone is toxic for human being. Specifically, it is irritative to skin, eyes and mucosa, casing headaches, dizziness and fatigue. In addition, long-term exposure can also cause illness and even death.[2–4] Thus, it is necessary to find an effective way to detect acetone.

Right now, various metal oxide semiconductors including MoO_3,[5] SnO_2,[6] ZnO,[7] Co_3O_4,[8] WO_3,[9] $ZnSnO_3$,[10] Zn_2SnO_4[11] and $ZnFe_2O_4$[12] are often used as sensitive materials because of their low cost, easy synthesis and good sensing performance. Among them, $ZnSnO_3$ has been applied in many fields, such as thin-film transistors,[13] photocatalyst[14] and piezoelectric generator.[15] Recently, it began to be used in gas sensors because of its structural advantages.[10] In gas sensing field, it is now generally accepted that sensing properties of sensing materials is based heavily on their microstructure and electronic structure.[16,17] Thus, reasonable constructing of the microstructure becomes an important method to enhance gas sensing performance of metal oxide semiconductors. Up to now, researchers have synthesized various $ZnSnO_3$ with different morphologies. For instance, Zhou *et al.* synthesized multi-shelled $ZnSnO_3$ hollow cubes via a facile co-precipitation approach, which exhibited high response values of 37.2 to 100 ppm formaldehyde.[18] Wang *et al.* prepared two dimensional (2D) $ZnSnO_3$ nanosheets using a graphene oxide (GO)-assisted way and the $ZnSnO_3$ nanosheets exhibited high response values of 57 to 10 ppm formaldehyde at 100 °C.[19] Sa *et al.* obtained porous $ZnSnO_3$ nanocubes via a microwave-assisted hydrothermal method, which exhibited high responses of 57.5 to 100 ppm triethylamine.[20]

In addition, constructing heterostructure is a valid approach to maximize sensing performance of $ZnSnO_3$. In recent years, carbon nanotubes (CNTs) have attracted many researcher's attention in gas sensing field due to their large specific surface area, high electron mobility and chemical stability.[21,22] However, pure CNTs usually exhibit low gas responses and bad selectivity, which limit their application in gas sensors. Fortunately, researchers have fabricated various CNTs/metal oxide semiconductor heterostructures and they showed good sensing properties. For instance, Zhang *et al.* prepared multi-walled carbon nanotubes (MWCNTs)/Co_3O_4 composites by a facile hydrothermal way and MWCNTs/Co_3O_4 composites showed good acetone sensing properties.[23] Jia *et al.* prepared flower-like α-Fe_2O_3/MWCNTs via a simple solvothermal way, which exhibited high response values (20.32) and short response time (2.3 s) at 220 °C.[24] Yang *et al.* synthesized MWCNTs/$NiWO_4$ microflowers via a simple co-precipitation way and the as-prepared products showed fast response/recovery speed (53 s/177 s) to 50 ppm NH_3.[25] Thus, it is expected that MWCNTs/$ZnSnO_3$ heterostructures show excellent acetone sensing performance.

Herein, MWCNTs/$ZnSnO_3$ heterostructures are synthesized by a simple hydrothermal process. The test results show that MWCNTs/$ZnSnO_3$ heterostructures exhibit not only

[†]Corresponding author. E-mail: 495431287@qq.com

© 2023 Chinese Physical Society and IOP Publishing Ltd

high responses of 24.1 and rapid response/recovery time of 1 s/9 s to 100 ppm acetone, but also relatively good repeatability and long-term stability. Thus, the as-obtained MWCNTs/$ZnSnO_3$ heterostructures are suitable materials for construction of high-performance acetone gas sensor.

2. Experimental details

2.1. Synthesis process

Figure 1 exhibits synthetic process of MWCNTs/$ZnSnO_3$. Typically, 5 mg of acidified MWCNTs, 0.5 mmol of $SnCl_4{\cdot}5H_2O$ and 0.5 mmol of $Zn(NO_3)_2{\cdot}6H_2O$ were dissolved into 30 mL of deionized water by vigorously stirring for 0.5 h. Then, $NH_3{\cdot}H_2O$ was added to the above solution to adjust to the PH to 11. Next, the solution was transferred to a 50 mL of teflon-lined stainless steel autoclave and maintained at 160 °C for 15 h. Finally, the samples were rinsed with deionized water and absolute ethanol, and then dried by 60 °C for 12 h. For comparison, pure $ZnSnO_3$ was synthesized by the similar method without the addition of MWCNTs.

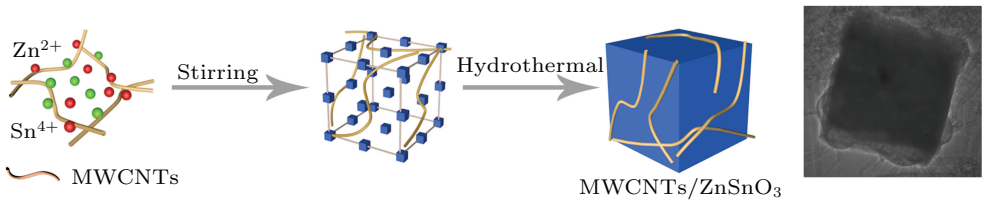


Fig. 1. The synthetic process of MWCNTs/$ZnSnO_3$.

2.2. Characterization

The x-ray diffraction (XRD) spectrum of the products was characterized by a Rigaku D/max-2500 diffractometer with Cu-$K\alpha_1$ radiation ($\lambda = 1.54056$ Å). The morphology and microstructure of the products were characterized with field-emission scanning electron microscopy (FESEM, Magellan 400) and transmission electron microscopy (TEM, JEM-2200FS). The surface compositions and bonding states of the samples were investigated by x-ray photoelectron spectroscopy (XPS, ESCALAB MKII).

2.3. Gas sensors fabrication and measurement

The process of fabricating sensors was systematically described in previous work.[26,27] In short, firstly, the sensitive slurry was obtained by mixing absolute ethanol and sensing materials. The slurry was coated on the surface of ceramic tube, on which a pair of gold electrodes and four Pt conducting wires were pre-installed. Then a Ni–Cr alloy coil was inserted into the tube to control the working temperature of gas sensor (Fig. 2) by adjusting the heating current. Before test, the as-obtained gas sensor required to be aged at 280 °C for two days.

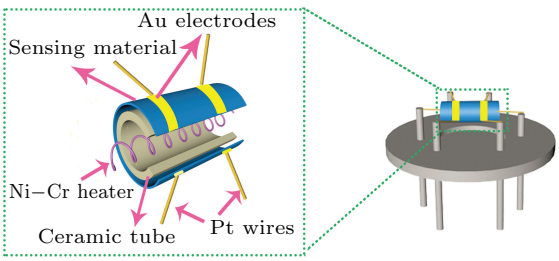


Fig. 2. The schematic illustration of gas sensor.

The sensing properties of the as-obtained gas sensor were investigated by using a CGS-8 intelligent gas sensing analysis system. The sensor responses were defined as R_a/R_g, where R_a and R_g were the sensor resistance under air and test gas, respectively. The response and recovery time were defined as the time taken by the sensor resistance to obtain 90% of total resistance variation in the case of response and recovery, respectively.

3. Results and discussion

3.1. Morphology and composition analysis

Figure 3 is the XRD pattern of the products. For pure MWCNTs, a diffraction peak at around 26 °C can be detected obviously, which is ascribed to the (002) plane of graphitic carbon (JCPDS No. 41-1487).

For pure $ZnSnO_3$ sample, its diffraction peaks correspond well to the standard $ZnSnO_3$ phase (JCPDS No. 11-274). For MWCNTs/$ZnSnO_3$ sample, its diffraction peaks are similar to that of pure $ZnSnO_3$ sample and no other peaks are observed, indicating that MWCNTs/$ZnSnO_3$ sample has high purity. Furthermore, the diffraction peak of MWCNTs are not detected, probably because of their relatively low content and low intensity of diffraction peak compared to the $ZnSnO_3$.[28,29]

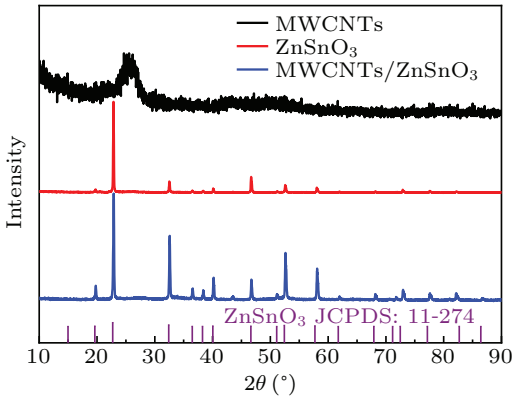


Fig. 3. The XRD pattern of the as-obtained samples.

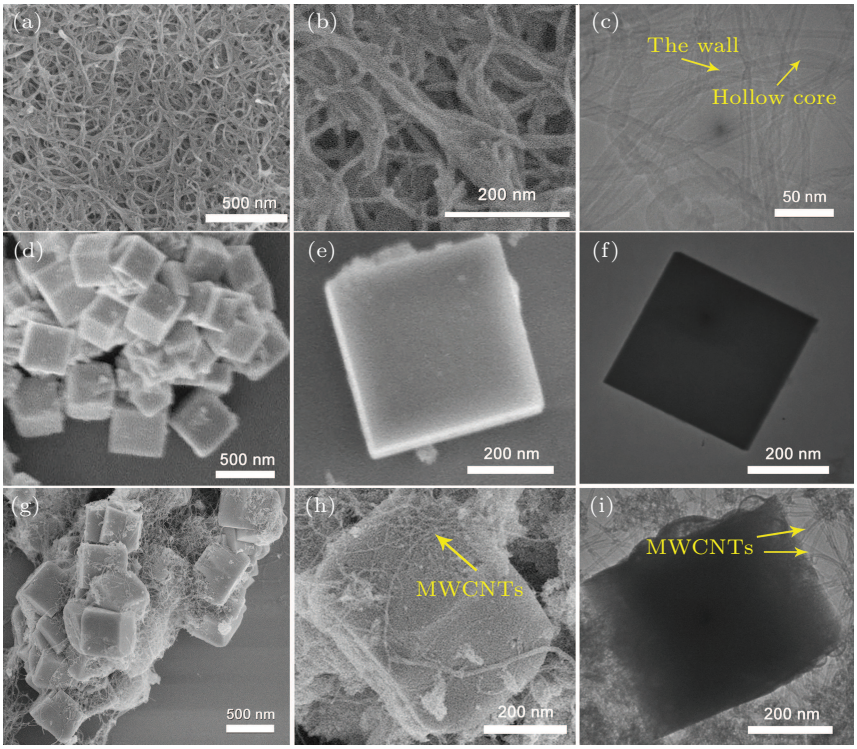


Fig. 4. The FESEM images of (a), (b) pure MWCNTs, (d), (e) $ZnSnO_3$ and (g), (h) MWCNTs/$ZnSnO_3$. The TEM images of (c) pure MWCNTS, (f) $ZnSnO_3$ and (i) MWCNTs/$ZnSnO_3$.

Figures 4(a)–4(c) are the FESEM and TEM images of pure MWCNTs. Clearly, many MWCNTs are observed and their surfaces are smooth. In addition, the difference between light and dark demonstrates the nanotube structure of MWCNTs. Figures 4(d) and 4(e) are the FESEM images of pure $ZnSnO_3$ sample. There are a lot of uniform nanocubes with the edge length of around 400 nm. From TEM image of pure $ZnSnO_3$ sample, solid cube structure can be observed (Fig. 4(f)). For MWCNTs/$ZnSnO_3$ sample, we can clearly see that many MWCNTs are attached to the surface of $ZnSnO_3$ nanocubes, demonstrating the formation of MWCNTs/$ZnSnO_3$ heterostructures (Figs. 4(g)–4(i)).

The microstructure of MWCNTs/$ZnSnO_3$ sample is further characterized by TEM. Obviously, MWCNTs have adhered to the surface of $ZnSnO_3$ nanocube, which also indicates the creation of MWCNTs/$ZnSnO_3$ heterostructures (Figs. 5(a) and 5(b)). The HRTEM image of MWCNTs/$ZnSnO_3$ sample is shown in Fig. 5(c). The interplanar spacing is 0.28 nm for the (220) plane of $ZnSnO_3$ and 0.34 nm for the (002) plane of MWCNTs, which also indicates the formation of MWCNTs/$ZnSnO_3$ heterostructures.

The compositions and surface chemical states of MWCNTs/$ZnSnO_3$ heterostructures and pure $ZnSnO_3$ sample are analyzed by XPS. Figures 6(a) and 6(b) are the Zn 2p spectra of pure $ZnSnO_3$ and MWCNTs/$ZnSnO_3$ heterostructures, respectively. Two peaks at 1022.4 eV and 1045.3±0.1 eV are detected, which are indexed to Zn $2p_{3/2}$ and Zn $2p_{1/2}$, respectively.[30,31] The results exhibit a normal state of Zn^{2+} in pure $ZnSnO_3$ and MWCNTs/$ZnSnO_3$ heterostructures. Figures 6(c) and 6(d) show the Sn 3d spectra of pure $ZnSnO_3$ and MWCNTs/$ZnSnO_3$ heterostructures, respectively. The peaks

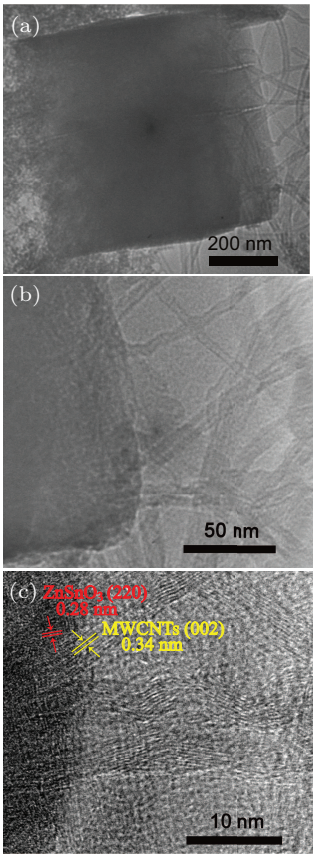


Fig. 5. (a), (b) The TEM and (c) HRETEM images of MWCNTs/$ZnSnO_3$.

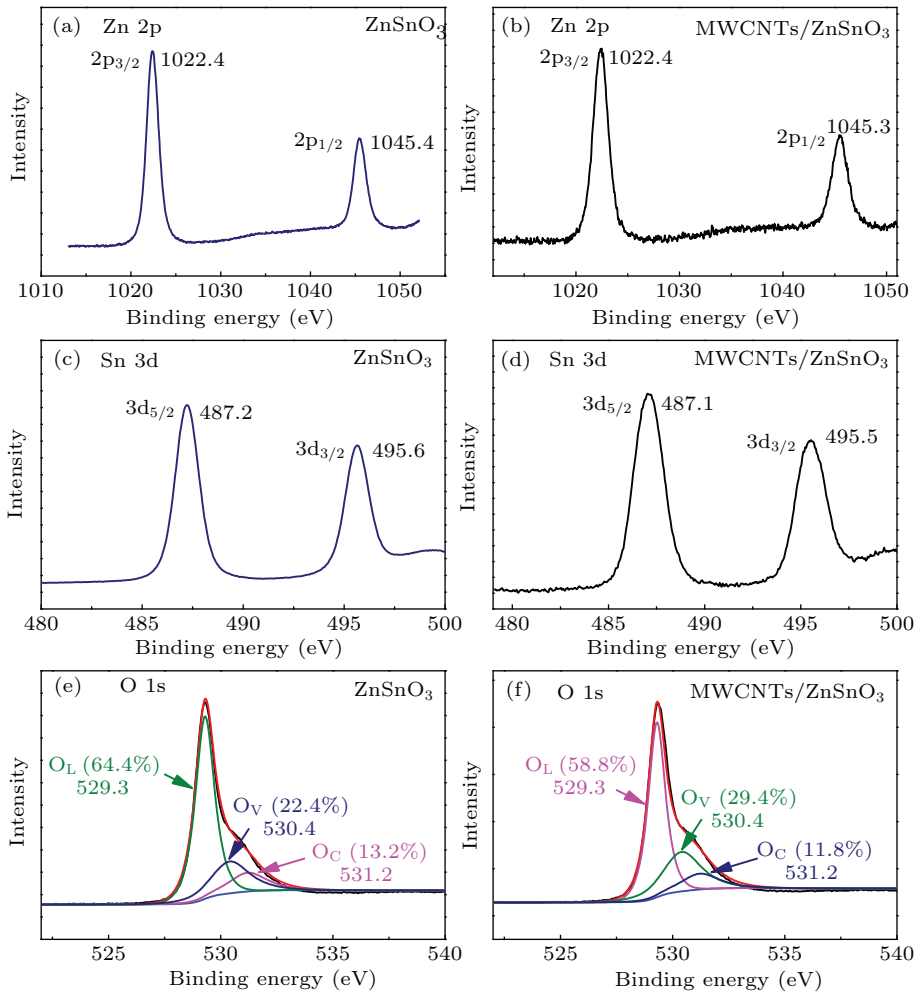


Fig. 6. (a) The Zn 2p, (c) Sn 3d and (e) O 1s spectra of pure $ZnSnO_3$; (b) the Zn 2p, (d) Sn 3d and (f) O 1 s spectra of MWCNTs/$ZnSnO_3$.

at 487.1±0.1 eV and 495.5 eV corresponding to Sn $3d_{5/2}$ and Sn $3d_{3/2}$, respectively, demonstrating a normal state of Sn^{4+} in pure $ZnSnO_3$ and MWCNTs/$ZnSnO_3$ heterostructures.[32] The O 1s spectra of pure $ZnSnO_3$ and MWCNTs/$ZnSnO_3$ heterostructures is shown in Figs. 6(e) and 6(f). It is obvious that both O 1s peaks are asymmetric, which can be decomposed into three peaks. The peaks at 529.3 eV, 530.4 eV and 531.2 eV belong to lattice oxygen (O_L), oxygen vacancies (O_V) and chemisorbed oxygen (O_C), respectively.[33–35] It is found that the relative proportion of oxygen vacancies in pure $ZnSnO_3$ and MWCNTs/$ZnSnO_3$ heterostructures is 22.4% and 29.4%, respectively. The results show MWCNTs/$ZnSnO_3$ heterostructures have more oxygen vacancies compared with the pure $ZnSnO_3$ sample and thus enhance their sensing performance.

3.2. Gas sensing properties

To investigate the optimal operating temperature, the gas response values of the samples to 100 ppm acetone are measured under working temperature ranging from 160 °C to 300 °C (Fig. 7(a)). Obviously, pure MWCNTs show extremely low response values at the working temperature of 160 °C–300 °C. For pure $ZnSnO_3$ and MWCNTs/$ZnSnO_3$ samples, they show the same trends. Specifically, the responses increase with the increasing of working temperature, and the responses obtain maximum at the working temperature of 260 °C. Then the responses decrease with the increasing of working temperature. Thus, the optimal working temperature of both pure $ZnSnO_3$ and MWCNTs/$ZnSnO_3$ samples is 260 °C. In addition, compared to pure $ZnSnO_3$, the responses of MWCNTs/$ZnSnO_3$ exhibits higher response values, which indicate that the formation of MWCNTs/$ZnSnO_3$ heterostructures enhances corresponding acetone sensing properties.

The responses of pure MWCNTs, $ZnSnO_3$ and MWCNTs/$ZnSnO_3$ to 100 ppm all kinds of testing gases at 260 °C are shown in Fig. 7(b). It is found that pure MWCNTs show an extremely low response values to all VOCs, indicating their bad selectivity. The responses of MWCNTs/$ZnSnO_3$ to 100 ppm of ethanol, acetone, benzene, toluene, methanol and ammonia are 16.1, 24.1, 10.2, 14.5, 7.7 and 5.4, respectively. The responses ratio of acetone to ethanol in MWCNTs/$ZnSnO_3$ is about 1.5 and that for pure $ZnSnO_3$ is about 1.35, indicating its enhanced selectivity.

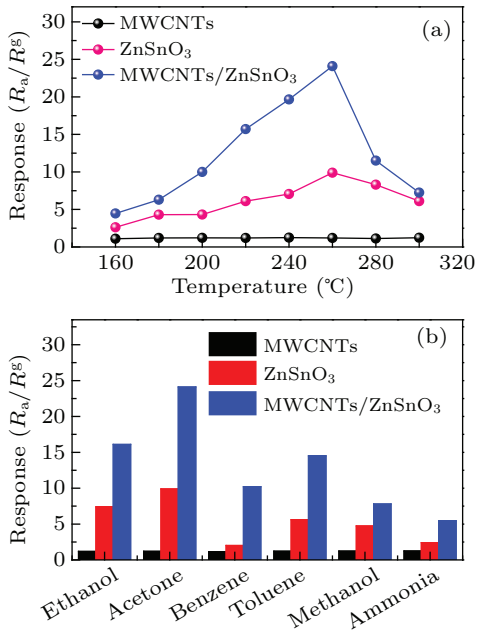


Fig. 7. (a) The gas responses of pure MWCNTs, $ZnSnO_3$ and MWCNTs/$ZnSnO_3$ to 100 ppm acetone are measured at 160 °C–300 °C. (b) The gas responses of pure MWCNTs, $ZnSnO_3$ and MWCNTs/$ZnSnO_3$ to 100 ppm different test gases at 260 °C.

Figures 8(a) and 8(b) are the responses of pure $ZnSnO_3$ and MWCNTs/$ZnSnO_3$ samples toward different concentrations of acetone (0.5 ppm–1000 ppm) at 260 °C, respectively. The responses of pure $ZnSnO_3$ sample for 10, 20, 50, 100, 200, 500 and 1000 ppm acetone are recorded as 1.2, 2.8, 5.6, 9.9, 16.5, 18.0 and 42.9, respectively. For MWCNTs/$ZnSnO_3$ sample, the responses to 0.5, 1, 5, 10, 20, 50, 100, 200, 500 and 1000 ppm acetone are 1.3, 1.8, 2.3, 3.2, 4.2, 13.6, 24.1, 45.9, 95.7 and 116.5, respectively. The corresponding relationship between gas responses and acetone concentration is shown in Fig. 8(c). It is found that the responses of MWCNTs/$ZnSnO_3$ sample depend near linearly on the acetone concentration ranging from 0.5 ppm to 500 ppm, demonstrating it is suitable for the acetone sensor.

Figure 8(d) exhibits the response/recovery speed of MWCNTs/$ZnSnO_3$ sample to 100 ppm acetone at 260 °C. Obviously, its response and recovery time are 1 s and 9 s, respectively. With such speedy response/recovery, the gas sensor is beneficial to realize real time detection. The repeatability of MWCNTs/$ZnSnO_3$ sample is shown in Fig. 8(e). The responses basically maintain the initial values upon nine successive measurements to 100 ppm acetone at 260 °C, indicating its relatively good repeatability. Figure 8(f) exhibits the long-term stability of MWCNTs/$ZnSnO_3$ sample. Clearly, the responses do not change distinctly for two months, demonstrating its relatively good long-term stability.

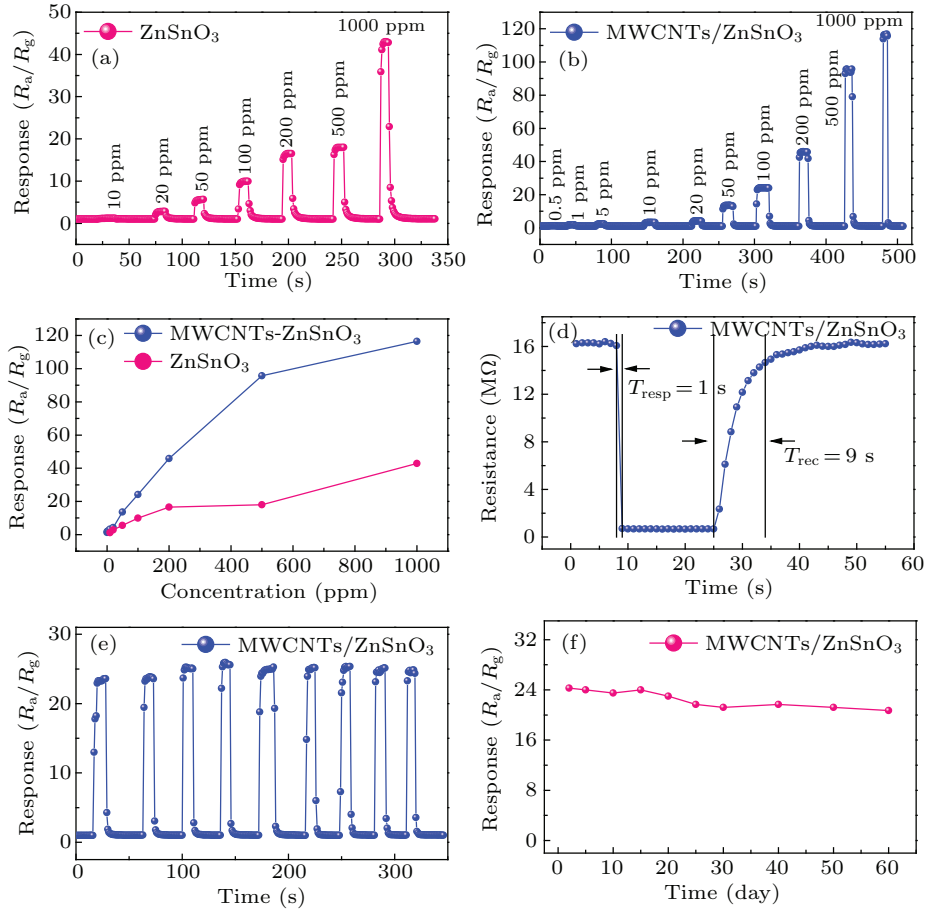


Fig. 8. The responses of (a) pure $ZnSnO_3$ and (b) MWCNTs/$ZnSnO_3$ samples toward different concentrations of acetone (0.5 ppm–1000 ppm). (c) The corresponding relationship between gas responses and acetone concentration of pure $ZnSnO_3$ and MWCNTs/$ZnSnO_3$. (d) The response/recovery speed of MWCNTs/$ZnSnO_3$ sample to 100 ppm acetone at 260 °C. (e) The repeatability and (f) long-term stability of MWCNTs/$ZnSnO_3$ sample.

Table 1. A comparison between the gas sensing properties of MWCNTs/$ZnSnO_3$ sensor and reported $ZnSnO_3$ based sensors.

Sample	Acetone (ppm)	LOD (ppm)	t_{res}/t_{rec} (s)	T (°C)	Response	Ref.
$ZnSnO_3$ hollow polyhedrons	~	~	17/10	240	12.5	[36]
Porous $ZnSnO_3$ cubes	100		–/–	300	16	[37]
$ZnSnO_3$ nanosheets	50	~	0.2/2.6	440	41	[38]
$ZnSnO_3$ nanoparticles	100	~	–/–	300	26	[39]
$ZnSnO_3/SnO_2$ microcubes	50	1	4/6	260	19.1	[40]
$ZnSnO_3/SnO_2$ hollow urchin	50	~	3/11	280	17	[41]
MWCNTs/$ZnSnO_3$ heterostructures	100	0.5	1/9	260	24.1	this work

Table 1 summarizes a comparison between the gas sensing properties of MWCNTs/$ZnSnO_3$ sensor and reported $ZnSnO_3$ based sensors.[36–41] Obviously, the MWCNTs/$ZnSnO_3$ sensor shows high responses, rapid response/recovery speed and low detection limit to acetone.

3.3. Gas sensing mechanism

At present, for the gas sensing of metal oxide semiconductors, the most widely accepted mechanism is based on the change in resistance of sensing materials in the adsorption and desorption process.[42,43] And $ZnSnO_3$ is an important n-type semiconductor. When $ZnSnO_3$ is exposed to air, oxygen molecules are adsorbed on the $ZnSnO_3$ surface and covert into different forms of oxygen ions (O_2^-, O^- and O^{2-}) by trapping the electrons from the conduction band of $ZnSnO_3$ (Eqs. (1)–(4)). Therefore, $ZnSnO_3$ material shows high resistance values in air. When $ZnSnO_3$ is exposed to acetone, oxygen ions (O^-) will react rapidly with the acetone, and forms H_2O, CO_2 and free electrons (Eq. (5)). These free electrons will return to the conduction band of $ZnSnO_3$. Thus, $ZnSnO_3$ material shows low resistance values in acetone (Fig. 9).

$$O_{2(gas)} \rightarrow O_{2(ads)}, \tag{1}$$

$$O_{2(ads)} + e^- \rightarrow O^-_{2(ads)}, \quad (T < 100\ ^\circ C), \tag{2}$$

$$O^-_{2(ads)} + e^- \rightarrow 2O^-_{(ads)}, \quad (100\ ^\circ C < T < 300\ ^\circ C), \tag{3}$$

$$O^-_{(ads)} + e^- \rightarrow O^{2-}_{(ads)}, \quad (T > 300\ ^\circ C), \tag{4}$$

$$CH_3COCH_{3(ads)} + 8O^-_{(ads)} \rightarrow 3CO_2 + 3H_2O + 8e^-. \tag{5}$$

From the gas sensing tests, MWCNs/$ZnSnO_3$ exhibits better acetone sensing performance compared with pure MWCNTs and $ZnSnO_3$, which are ascribed to the following factors.

Firstly, the formation of MWCNTs/$ZnSnO_3$ heterostructures improves the sensing properties. MWCNTs are a typical p-type semiconductor material. However, $ZnSnO_3$ is an important n-type semiconductor material. When MWCNTs are attached to the surface of $ZnSnO_3$ material, p–n heterostructures will be generated at the interface of MWCNTs and $ZnSnO_3$. At the same time, because of their different Fermi level, electrons will be transferred from $ZnSnO_3$ to MWCNTs and holes transfer in opposite direction to equilibrate the Fermi energy level, which form a built-in electric field. Thus, the thicker depletion layer is also created, resulting in the increasing of MWCNTs/$ZnSnO_3$ resistance in air. When MWCNTs/$ZnSnO_3$ heterostructures are exposed to acetone, the electrons will be released back to $ZnSnO_3$. It is reported that MWCNTs can accept the electrons and play a good medium role for carrier mobility due to their excellent conductivity and high electron mobility, leading to further decreases in resistance of MWCNTs/$ZnSnO_3$ heterostructures.[24] Thus, gas sensing performance of MWCNTs/$ZnSnO_3$ heterostructures including response values and response/recovery speed will be improved. In addition, functionalization of MWCNTs promotes the chemical reaction of material surface, resulting in the enhancement of gas responses.[44]

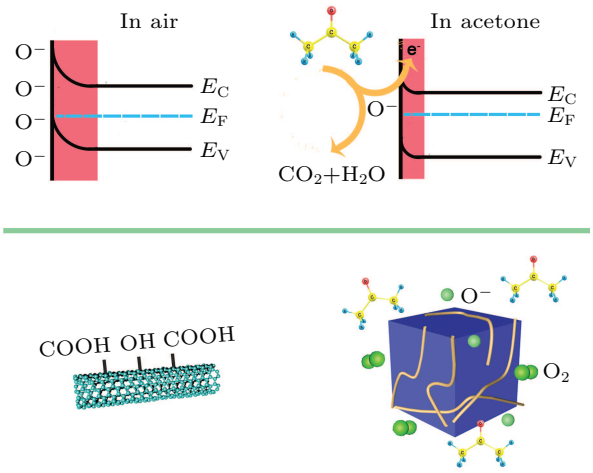


Fig. 9. The gas sensing mechanism of MWCNTs/$ZnSnO_3$ sample.

Secondly, the formation of MWCNTs/$ZnSnO_3$ heterostructures can introduce the lattice mismatch because of different lattice constants between MWCNTs and $ZnSnO_3$, which will bring about lattice deformation at the interface.[45,46] Meanwhile, oxygen vacancies will spontaneously generate at the interface to adapt to lattice deformation during the formation of MWCNTs/$ZnSnO_3$ heterostructures.[47] Thus, MWCNTs/$ZnSnO_3$ heterostructures possess more oxygen vacancies compared with pure $ZnSnO_3$ sample, which are consistent with XPS analysis. Oxygen vacancies can act as electron donors and help to create more oxygen ions on the surface of sensing material, which contribute to the surface oxidation-reduction reaction.[48,49] Therefore, the sensing performance of MWCNTs/$ZnSnO_3$ heterostructures enhances correspondingly.

4. Conclusion

In this work, MWCNTs/$ZnSnO_3$ heterostructures are prepared through a simple hydrothermal method. Then gas sensing properties of sensing materials are investigated in detail. It is found that the gas sensing performance of MWCNTs/$ZnSnO_3$ is far superior than that of pure MWCNTs and $ZnSnO_3$ sample. In particular, MWCNTs/$ZnSnO_3$ heterostructures show not only high response values of 24.1 and fast response/recovery speed (1 s/9 s) to 100 ppm acetone at 260 °C, but also relatively good repeatability and long-term stability. In addition, this work provides experimental and theoretical basis for synthesis of high-performance MWCNT-based chemical sensors.

Acknowledgements

Project supported by Fundamental Research Program of Shanxi Province, China (Grant No. 202103021223004) and Fundamental Research Fund of Taiyuan University (Grant No. 21TYKQ21).

References

[1] Zhang X M, Dong Z J, Liu S R, Shi Y, Dong Y H and Feng W 2017 *Sens. Actuators B* **243** 1224
[2] Righettoni M, Tricoli A and Pratsinis S E 2010 *Anal. Chem.* **82** 3581
[3] Deng C H, Zhang J, Yu X F, Zhang W and Zhang X M 2004 *J. Chromatogr. B* **810** 269
[4] Zhang J Z and Yan Y 2017 *J. Mater. Sci.* **52** 13711
[5] Wei Q, Song P, Li Z Q, Yang Z X and Wang Q 2019 *Vacuum* **162** 85
[6] Wang Z, Fan S X and Tang W 2022 *Chin. Phys. B* **31** 028101
[7] Li Y Z, Feng Q J, Shi B, Gao C, Wang D Y and Liang H W 2020 *Chin. Phys. B* **29** 018102
[8] Cao J, Zhang N R, Wang S M and Zhang H M 2020 *J. Colloid. Interf. Sci.* **577** 19
[9] Du L Y, Xiao P D, Liu Y, Zhai C B, Wang D X and Zhang M Z 2020 *J. Alloys Compd.* **828** 154463
[10] Yin Y Y, Shen Y B, Zhou P F, Lu R, Li A, Zhao S K, Liu W G, Wei D Z and Wei K F 2020 *Appl. Surf. Sci.* **509** 145335
[11] Wang T L, Wang X D, Wang Y, Yi G Y, Shi C, Yang Y Q, Sun G and Zhang Z Y 2022 *Mater. Sci. Semicond. Process.* **140** 106403
[12] Zhai C B, Zhao Q, Gu K K, Xing D J and Zhang M Z 2019 *J. Alloys Compd.* **784** 660
[13] Rong A, Gao X P, Li G R, Yan T Y, Zhu H Y, Qu J Q and Song D Y 2006 *J. Phys. Chem. B* **110** 14754
[14] Chen J, Luo W S, Yu S J, Yang X X, Wu Z, Zhang H F, Gao J, Mai Y W, Li Y X and Jia Y M 2020 *Ceram. Int.* **46** 9786
[15] Wu J M, Xu C, Zhang Y, Yang Y, Zhou Y and Wang Z L 2012 *Adv. Mater.* **24** 6094
[16] Lee J H 2009 *Sens. Actuators B* **140** 319
[17] Barsan N, Koziej D and Weimar U 2007 *Sens. Actuators B* **121** 18
[18] Zhou T T, Zhang T, Zhang R, Lou Z, Deng J N and Wang L L 2017 *ACS Appl. Mater. Interfaces* **9** 14525
[19] Wang D, Pu X X, Yu X, Bao L P, Cheng Y, Xu J C, Han S N, Ma Q X and Wang X Y 2022 *J. Colloid. Interf. Sci.* **608** 1074
[20] Sa B S, Zito C A, Perfecto T M and Volanti D P 2021 *Sens. Actuators B: Chem.* **338** 129869
[21] Bandal H A, Jadhav A R, Chaugule A A, Chung W J and Kim H 2016 *Electrochim. Acta* **222** 1316
[22] Dai M, Zhao L, Gao H, Sun P, Liu F, Zhang S, Shimanoe K, Yamazoe N and Lu G Y 2017 *ACS Appl. Mater. Interfaces* **9** 8919
[23] Zhang R, Zhang M, Zhou T T and Zhang T 2018 *Inorg. Chem. Front.* **5** 2563
[24] Jia X H, Cheng C D, Yu S W, Yang J, Li Y and Song H J 2019 *Sens. Actuators B* **300** 127012
[25] Yang M, Au C T, Deng G W, Mathur S Y, Huang Q P, Luo X L, Xie G Z, Tai H L, Jiang Y D, Chen C X, Cui Z, Liu X Y, He C Z, Su Y J and Chen J 2021 *ACS Appl. Mater. Interfaces* **13** 52850
[26] Yang T Y, Gu K K, Zhu M M, Lu Q, Zhai C B, Zhao Q, Yang X D and Zhang M Z 2019 *Sens. Actuators B* **279** 410
[27] Du L Y, Gu K K, Zhu M M, Zhang J and Zhang M Z 2019 *Sens. Actuators B* **288** 298
[28] Zhang Y C, Gao S T and Xing H L 2019 *J. Alloys Compd.* **777** 544
[29] Rosehr A, Griebe D and Luinstra G A 2018 *Compos. Sci. Technol.* **156** 28
[30] Jia X H, Tian M G, Dai R R, Lian D D, Han S, Wu X Y and Song H J 2017 *Sens. Actuators B* **240** 376
[31] Wang L L, Tang K B, Liu Z P, Wang D K, Sheng J and Cheng W 2011 *J. Mater. Chem.* **21** 4352
[32] Wang Y D and Cheng T 2009 *Electrochim. Acta* **54** 3510
[33] Ding H, Zhu J H, Jiang J, Ding R M, Feng Y M, Wei G M and Huang X T 2012 *RSC Adv.* **2** 10324
[34] Zhang G C, Han X, Bian W W, Zhan J H and Ma X C 2016 *RSC Adv.* **6** 3919
[35] Bai S L, Tian Y, Zhao Y H, Fu H, Tang P G, Luo R X, Li D Q, Chen A F and Li C C 2018 *Sens. Actuators B* **259** 908
[36] Chen Q, Ma S Y, Jiao H Y, Zhang G H, Chen H, Xu X L, Yang H M and Qiang Z 2017 *Ceram. Int.* **43** 1617
[37] Huang J R, Xu X J, Gu C P, Wang W Z, Geng B Y, Sun Y F and Liu J H 2012 *Sens. Actuators B* **171** 572
[38] Chen Y J, Yu L, Li Q, Wu Y, Li Q H and Wang T H 2012 *Nanotechnology* **23** 415501
[39] Lu L Z, Zhang A Q, Xiao Y H, Gong F L, Jia D Z and Li F 2012 *Mater. Sci. Eng. B* **177** 942
[40] Zhang J T, Jia X H, Lian D D, Yang J, Wang S Z, Li Y and Song H J 2021 *Appl. Surf. Sci.* **542** 148555
[41] Lian D D, Shi B, Dai R R, Jia X H and Wu X Y 2017 *J. Nanopart. Res.* **19** 401
[42] Yang D J, Kamienchick I, Youn D Y, Rothschild A and Kim I D 2010 *Adv. Funct. Mater.* **20** 4258
[43] Yang T Y, Yu H, Xiao B X, Li Z F and Zhang M Z 2017 *J. Alloys Compd.* **699** 921
[44] Sin M, Chow G, Wong G, Li W, Leong P and Wong K 2007 *IEEE Trans. Nanotechnol.* **6** 571
[45] Wang Z H, Zhang K C, Fei T, Gu F B and Han D M 2020 *Sens. Actuators B* **318** 128191
[46] Kim J H, Lee J H, Mirzaei A, Kim H W and Kim S S 2017 *Sens. Actuators B* **248** 500
[47] Yang Y, Zhao S H, Bi F K, Chen J F, Wang Y X, Cui L F, Xu J C and Zhang X D 2022 *Appl. Catal. B* **315** 121550
[48] Wu J J, Huang Q W, Zeng D W, Zhang S P, Yang L, Xia D S, Xiong Z D and Xie C S 2014 *Sens. Actuators B* **198** 62
[49] Qin Y X and Ye Z H 2016 *Sens. Actuators B* **222** 499